THE BELL SYSTEM TECHNICAL JOURNAL
Vol. 57, No. 9, November 1978
Printed in U.S.A.

A Loss Model for Parabolic-Profile Fiber Splices

By C. M. MILLER and S. C. METTLER

(Manuscript received April 26, 1978)

In the past, measurement results of splice loss of optical fibers have corresponded poorly to existing theory, which assumes a uniform power distribution across the cone of radiation defined by the local numerical aperture. In this paper, a model is developed in which a Gaussian power distribution across the local numerical aperture is assumed. Transmission through a splice at each point on the transmitting core is found to depend on the ratio of receiving to transmitting numerical aperture at that point. Numerical integration of these "point" transmission functions over core areas of interest yields both splice loss and the additional loss that occurs in a long fiber following the splice. This model cannot be theoretically rigorous, since it is inconsistent with boundary conditions required by the laws of light propagation. However, it has been found to predict splice loss under varying conditions with much greater accuracy than existing theory. The model has the further virtue of being able to calculate how variations in many intrinsic and extrinsic splice parameters combine to produce an overall splice loss.

I. INTRODUCTION

Calculations for the loss in an optical fiber splice, as a function of offset, tilt, diameter, or numerical aperture mismatch, have been reported by several authors.[1–3] These calculations all assumed a uniform power distribution across the cone of radiation defined by the local numerical aperture (NA). This is consistent with assuming equal mode excitation, equal mode attenuation, and no mode coupling.[4] An assumption concerning the power distribution is necessary to characterize all combinations of both intrinsic and extrinsic splice imperfections. While these assumptions allow easy calculations, correspondence with measurement data has been unacceptable.[3] Gloge[5] reported results based on a diffusion process from the uniform power distribution to the steady-state distribution calculated by Marcuse.[6] Correspondence with

measurement data is much improved for the case of small offsets; however, approximations used in the theory make it difficult to characterize other splice imperfections or splice loss for large offsets.

This paper presents a phenomenological model with an assumed power distribution selected solely due to resulting correspondence of calculated effects of splice imperfections with measurement data. The model is not intended for uses other than splice loss characterization, and since the model does not obey the laws of ray optics exactly, caution should be exercised in any other uses of it.

II. DETAILS OF THE MODEL

The power distribution across the cone of radiation defined by the numerical aperture at any point on a fiber core is assumed to be Gaussian in form. Figure 1 is a sketch of the assumed radially symmetric distribution across the cone of radiation from a given point on the fiber core. The model consists of solving for the transmission ratio in terms of transmitting and receiving numerical apertures, then integrating this ratio over the core areas of interest.

Consider the steady-state power distribution across the cone defined by the local numerical aperture to be Gaussian in form, normalized to a value of 1 at $r = 0$.

$$p(r) = e^{-r^2/2\sigma^2}, \tag{1}$$

where σ is proportional to the width of the Gaussian.

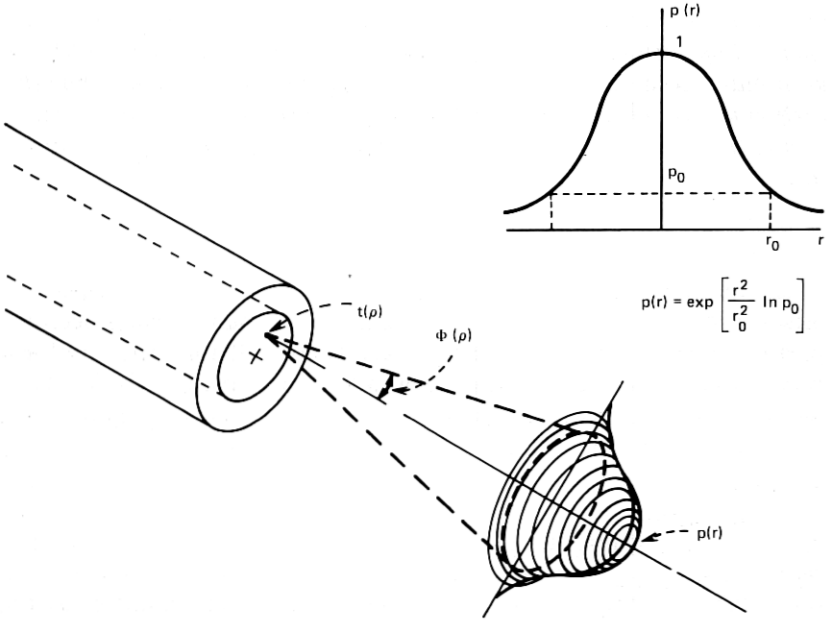

Fig. 1—Gaussian power distribution.

Numerical aperture has been defined by various investigators to be the $1/e^2$, 0.1 or 0.01 power level. This power level, p_0, determines the width of the Gaussian and will be left as a parameter. Therefore, at r_0,

$$p_0 = e^{-r_0^2/2\sigma^2} \tag{2}$$

or

$$p(r) = e^{(r^2/r_0^2)\ln p_0}. \tag{3}$$

III. NA MISMATCH

The application of this simple model can best be illustrated by considering the change in the power distribution as it propagates through a splice. The usual class of circularly symmetric index of refraction profiles[4] is used throughout this paper. In this example, transmitting and receiving fiber profiles are identical except for the value of n_{01}. Therefore, the NA as a function of transmitting fiber core radius (ρ) is

$$\mathrm{NA}_1(\rho) \approx n_{01}\sqrt{2\Delta_1}\left[1 - \left(\frac{\rho}{R}\right)^{\alpha}\right]^{1/2}, \tag{4}$$

where $\Delta_1 \approx (n_{01} - n_c)/n_{01}$ is small
n_{01} = refractive index at center of core
n_c = refractive index of cladding
α = 2 for nearly parabolic profile fibers
R = fiber core radius.

The angle $\phi_1(\rho)$ (Fig. 1) is determined by $\mathrm{NA}_1(\rho)$ to be

$$\phi_1(\rho) = \sin^{-1}\left[\mathrm{NA}_1(\rho)/n_1(\rho)\right], \tag{5}$$

where

$$n_1(\rho) = n_{01}\left[1 - 2\Delta_1\left(\frac{\rho}{R}\right)^{\alpha}\right]^{1/2}. \tag{5a}$$

The power distribution at a given value of ρ is assumed to be

$$p_1(r) = e^{(r^2/r_1^2)\ln p_0}, \tag{6}$$

where r_1 is proportional to tan ϕ_1 (Fig. 1).

For the receiving fiber, $\mathrm{NA}_2(\rho)$ will first be assumed to be less than the transmitting fiber $\mathrm{NA}_1(\rho)$, so that

$$p_2(r) = e^{(r^2/r_2^2)\ln p_0} \tag{7}$$

is the relative power distribution that corresponds to the same point on the receiving fiber. Figure 2 shows these two functions for $r_2 < r_1$ and for Gaussian distributions which are truncated at r_2 and r_1, respectively. Using these truncated distributions, we assume the power in region I is lost immediately at the splice, since power in this region lies totally outside the receiving NA. Splice transmission through this point is then

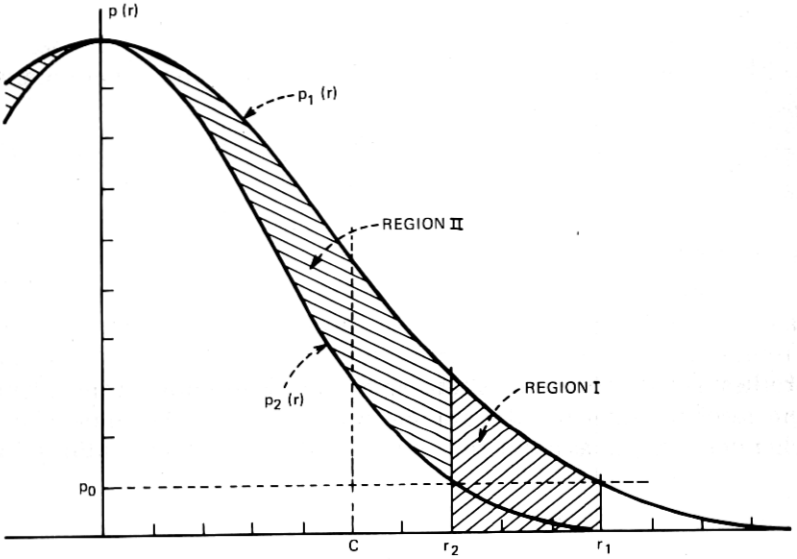

Fig. 2—Point transmission distributions.

$$t(\rho) = \frac{\int_0^{r_2} p_1(r)\, r dr}{\int_0^{r_1} p_1(r)\, r dr}, \tag{8}$$

$$t(\rho) = \frac{1}{p_0 - 1}\left[e^{(r_2/r_1)^2 \ln p_0} - 1\right] \tag{9}$$

for $r_2 < r_1$.

Since $r_1 = k \tan \phi_1$ and $r_2 = k \tan \phi_2$ where k is a constant of proportionality, then using (4) and (5),

$$\frac{r_2}{r_1} \approx \frac{\tan (\sin^{-1} \sqrt{2\Delta_2})}{\tan (\sin^{-1} \sqrt{2\Delta_1})} \approx \frac{\mathrm{NA}_2}{\mathrm{NA}_1} \tag{10}$$

for some given ρ.

For this particular example, $\mathrm{NA}_2/\mathrm{NA}_1$ is constant for every point (ρ) on the fiber core; therefore, eq. (9) gives the total transmission just after the splice for a truncated Gaussian distribution.

For the case of nontruncated Gaussian distributions, (8) and (9) become

$$t(\rho) = \frac{\int_0^{r_2} p_1(r)\, r dr + \int_{r_2}^{\infty} p_2(r)\, r dr}{\int_0^{\infty} p_1(r)\, r dr}, \tag{11}$$

$$t(\rho) = 1 + \left(\frac{r_2}{r_1}\right)^2 p_0 - e^{(r_2/r_1)^2 \ln p_0}, \tag{12}$$

for $r_2 < r_1$. For small values of p_0, (12) and (9) yield similar results. The full Gaussian is used to simplify later computations.

Since this example contains radially symmetric distributions, there is no dependence on θ. Equation (12) gives the transmission through the splice at a point for the steady-state power distribution assumed in (3). Again, for this example, $(r_2/r_1)^2$ is constant across the fiber core; therefore, (12) gives the total transmission just after the splice for a numerical aperture mismatch.

IV. COMPARISON WITH NA MISMATCH DATA

Equation (12) can be compared to measurement data for a splice with an NA mismatch ($r_2 < r_1$, receiving fiber NA < transmitting fiber NA). This transmission coefficient represents an immediate loss at the splice. Figure 3 contains measurement data along with calculations for both a uniform power distribution and a Gaussian distribution. The parameter, p_0, is set to $1/e^2$ and 0.1. As shown in Fig. 3, sensitivity to the value selected for p_0 is significant only for large NA mismatches.

Figure 3 contains data obtained using a HeNe and a GaAlAs laser source with a long input fiber (>500 m). Fibers selected for these measurements were well matched in O.D., core diameter, and α, but contained mismatches in NA. There were, however, slight differences in O.D., core diameter, and α on the order of a few percent, so that measured loss would be expected to differ somewhat from calculated values.

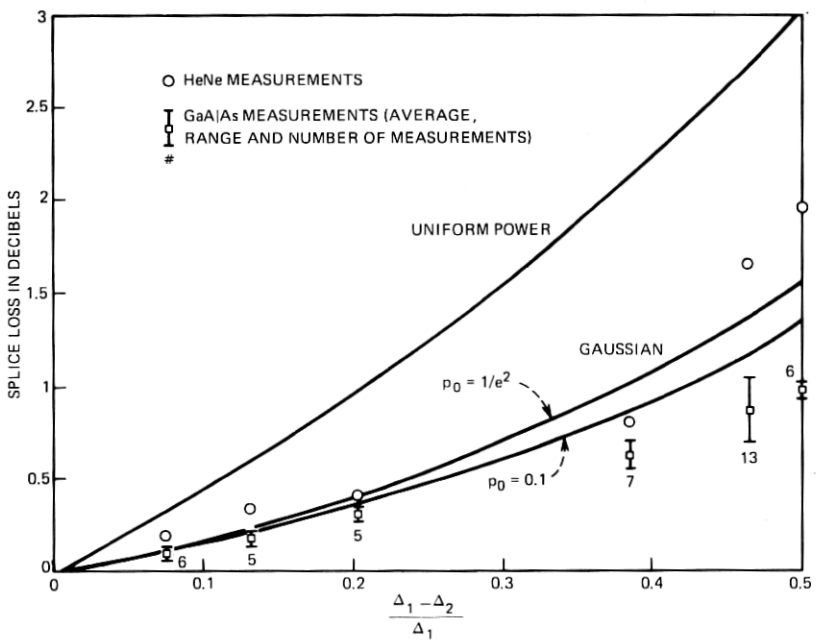

Fig. 3—Loss due to numerical aperture mismatch.

Correspondence with measured data using either source is good compared to the uniform power distribution model which predicts too much loss.

Before this model can be applied in general, the case of transmission from a smaller NA transmitting fiber to a larger NA receiving fiber must be considered. If, in Fig. 2, r_2 represents the transmitting fiber and r_1 the receiving fiber, then all the power contained in the cone of radiation defined by the transmitting NA is within the receiving NA. A unity transmission coefficient is assumed for this case.

V. NEAR-FIELD POWER DISTRIBUTION

The near-field power distribution as a function of core radius, ρ, can be calculated for the Gaussian model after a suitable weighting function is applied. Since a Gaussian distribution implies higher loss for higher order modes of propagation (the tails of the distribution), a weighting function is needed to reduce the amplitude of the Gaussian as a function of radius. This is required since only higher order modes of propagation are significant near the core-cladding interface. The weighting function assumed is the power distribution for the uniform power model. From (4),

$$P(\rho) \approx P_0 \left[1 - \left(\frac{\rho}{R}\right)^2\right] \tag{13}$$

for the case of uniform power across the cone of radiation defined by the numerical aperture where P_0 is proportional to Δ, n_0 and input power.[3] With this function used as the amplitude at $r = 0$, then

$$P(\rho) \approx P_0 \left(1 - \frac{\rho^2}{R^2}\right) \int_0^{2\pi} \int_0^{\infty} e^{(r/r_0)^2 \ln p_0} r \, dr \, d\theta. \tag{14}$$

Using (4) to obtain r_0,

$$P(\rho) \approx P_0(1 - \rho^2)^2 \tag{15}$$

where all constant terms have been combined in P_0 and $R = 1$.

VI. COMPARISON WITH NEAR-FIELD POWER MEASUREMENTS

Measurements of near-field power were made with a GaAlAs laser source after propagation through a long (>1 km) fiber wrapped under tension to simulate the effects of some microbending loss (~1 dB/km). These measurements were made using a 100X objective and a TV vidicon camera. Figure 4 is a photograph of the camera output for a typical Western Electric fiber. An approximation to the curve was obtained by smoothing over the index dip and averaging power measurements for each side of the distribution. Calculations using (13) for the uniform distribution and (15) are plotted for comparison. The calculated

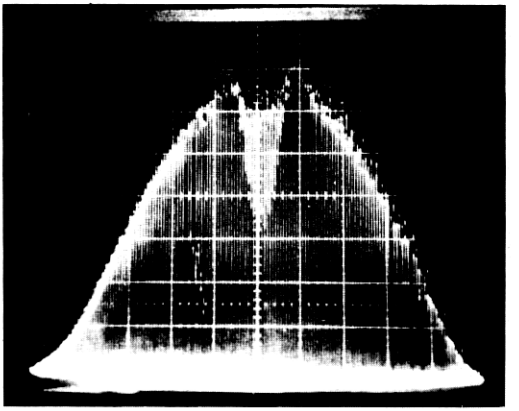

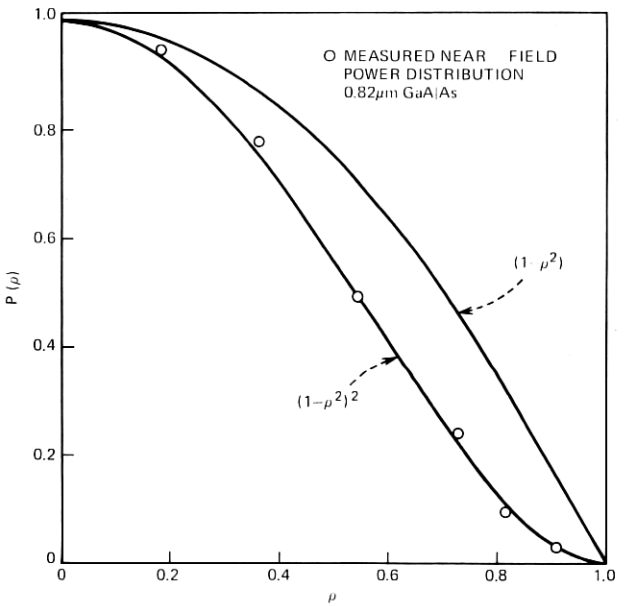

Fig. 4—Near-field power distribution.

steady-state power distribution using the Gaussian model with the $(1 - \rho^2)$ weighting function is in excellent agreement with the measured distribution.

VI. ADDITIONAL LOSS IN THE FIBER AFTER A SPLICE

A parabolic index fiber splice is known to cause additional loss in the fiber after the splice.[7] This additional loss depends on the differential mode attenuation and mode coupling characteristics of the receiving fiber and, for the fibers used in these experiments, is approximately equal to the loss at the splice for small offsets.[7] Therefore, any realistic description of an optical fiber splice must include this effect.

Referring to Fig. 2, the power in region II is seen to be within the numerical aperture of the receiving fiber; however, this power is improperly distributed. The sharp decrease in power at the edge of the receiving numerical aperture, r_2, is physically impossible; however, this effect is significantly reduced compared to the uniform power model. As this distribution propagates down the fiber length (l), we assume that a new Gaussian steady-state distribution will be generated, as shown in Fig. 5. Some portion, c, of the excess energy contained in region II of Fig. 2 will be lost in the process of reestablishing steady-state conditions. If energy couples to adjacent modes with equal probability and if all modes are equally excited and attenuated, then 1/2 of the power in region II would be lost during redistribution. Since the excess energy in region II is skewed toward higher order modes which may be lossier, c would be expected to be greater than 1/2. The loss mechanism is probably transfer of some of this excess energy to higher order propagating or leaky modes.[8]

Referring to Fig. 2, the equivalent transmission loss due to power lost from region II is

$$\Delta t(\rho) = \frac{c\left[\int_0^{r_2} p_1(r)\, r dr - \int_0^{r_2} p_2(r)\, r dr\right]}{\int_0^{\infty} p_1(r)\, r dr}. \tag{16}$$

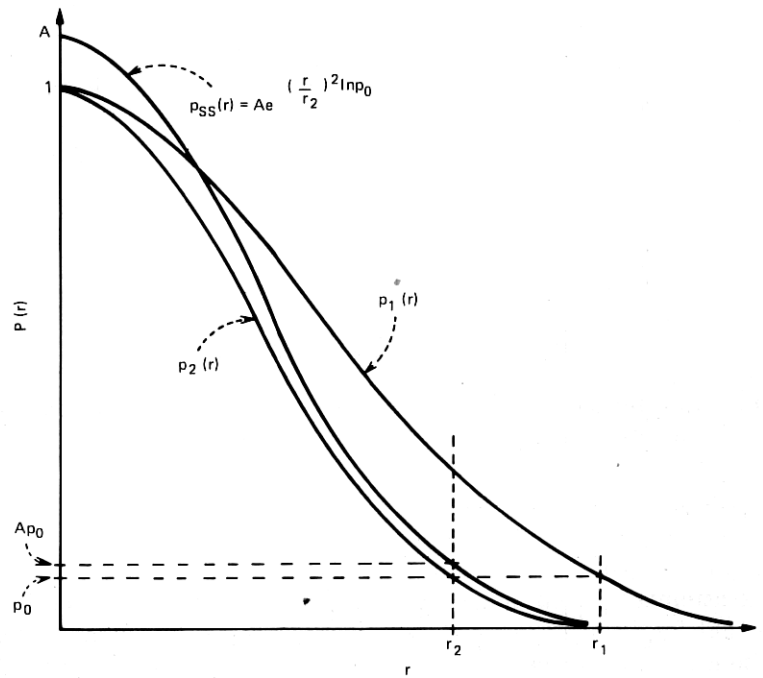

Fig. 5—Steady-state power distribution.

Evaluating this integral yields

$$\Delta t(\rho) = -ce^{(r_2/r_1)^2 \ln p_0} + c + c\left(\frac{r_2}{r_1}\right)^2 \cdot (p_0 - 1). \tag{17}$$

To approximate c, we use the centroid for the solid of revolution for region II in Fig. 2. This places one-half the excess energy in the region $0 < r < c$ and the remaining energy between $c < r < r_2$. This radius is taken as the value for c. From Fig. 2,

$$\int_0^c [p_1(r)\, rdr - p_2(r)\, rdr] = \int_c^{r_2} [p_1(r)\, rdr - p_2(r)\, rdr]. \tag{18}$$

Solving the integrals yields the following nonlinear equation:

$$e^{(c/r_1)^2 \ln p_0} - \left(\frac{r_2}{r_1}\right)^2 e^{(c/r_2)^2 \ln p_0} = \frac{1}{2}\left[1 + e^{(r_2/r_1)^2 \ln p_0} - \left(\frac{r_2}{r_1}\right)^2 (p_0 + 1)\right]. \tag{19}$$

This equation was solved for c/r_2 with $0 < r_2/r_1 < 1$ for $p_0 = 0.1$ and $p_0 = 1/e^2$, and found to be accurately approximated by a quadratic equation. For $p_0 = 0.1$,

$$c \approx 0.7994 - 0.08796 \left(\frac{r_2}{r_1}\right)^2 + 0.00846 \left(\frac{r_2}{r_1}\right)^4 \tag{20}$$

and for $p_0 = 1/e^2$,

$$c \approx 0.8041 - 0.0724 \left(\frac{r_2}{r_1}\right)^2 + 0.00636 \left(\frac{r_2}{r_1}\right)^4. \tag{21}$$

The total effect of the splice is then

$$t_{\text{tot}}(\rho) = t(\rho) - \Delta t(\rho). \tag{22}$$

$$t_{\text{tot}}(\rho) = (1 - c)\left[1 + p_0 \left(\frac{r_2}{r_1}\right)^2 - e^{(r_2/r_1)^2 \ln p_0}\right] + c\left(\frac{r_2}{r_1}\right)^2, \tag{23}$$

where $t(\rho)$ is the immediate point transmission coefficient at the splice given by (12) and $\Delta t(\rho)$ is the reduction in transmission due to power lost in reestablishing a steady-state Gaussian distribution in a long fiber after the splice given by (17). Again, we call attention to the fact that the value of c probably depends on the differential mode attenuation and mode coupling characteristics of the receiving fiber.

VIII. DIAMETER MISMATCH

The necessary parts of the model have been developed so that the effect of diameter mismatch (Fig. 6) can now be considered. Let the transmitting NA function equal

$$\text{NA}_1(\rho) = n_0 \sqrt{2\Delta}\left[1 - \left(\frac{\rho}{R_1}\right)^2\right]^{1/2} \tag{24}$$

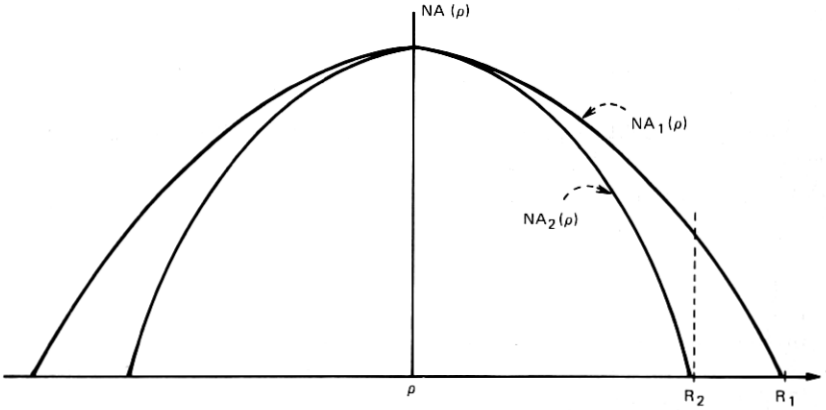

Fig. 6—Core index of refraction profiles for the case of diameter mismatch.

and the receiving NA function equal

$$\mathrm{NA}_2(\rho) = n_0 \sqrt{2\Delta} \left[1 - \left(\frac{\rho}{R_2}\right)^2\right]^{1/2}, \tag{25}$$

where R_1 and R_2 are the transmitting and receiving core radii. For $K = R_2/R_1$ and R_2 normalized to unity,

$$\left(\frac{r_2}{r_1}\right)^2 \simeq \frac{1-\rho^2}{1-K^2\rho^2}. \tag{26}$$

This ratio is not constant with ρ (except for $K = 1$), so that an integration over the receiving core is necessary. Distributions remain radially symmetric; therefore, no angle dependence is present.

$$T_{\mathrm{tot}} = \frac{\int_0^1 t(\rho)\,[1-K^2\rho^2]^2\,\rho d\rho}{\int_0^{1/K} [1-K^2\rho^2]^2\,\rho d\rho}, \tag{27}$$

where $t(\rho)$ equals eq. (12) for the effect at the splice, or by $t_{\mathrm{tot}}(\rho)$ [eq. (23)], to include the additional loss in the fiber after the splice. This integral must be solved by numerical techniques.

IX. COMPARISON WITH DIAMETER MISMATCH DATA

Figure 7 compares the calculations of short-length-diameter mismatch effects at the splice with measured results for various values of K. Fibers were drawn from the same preform to insure that α and NA mismatch were minimized. A HeNe laser source was used with approximately 1 m of fiber after the splice.

The Gaussian power distribution model shows good agreement with measurement data. Long-length-diameter mismatch data are not presently available.

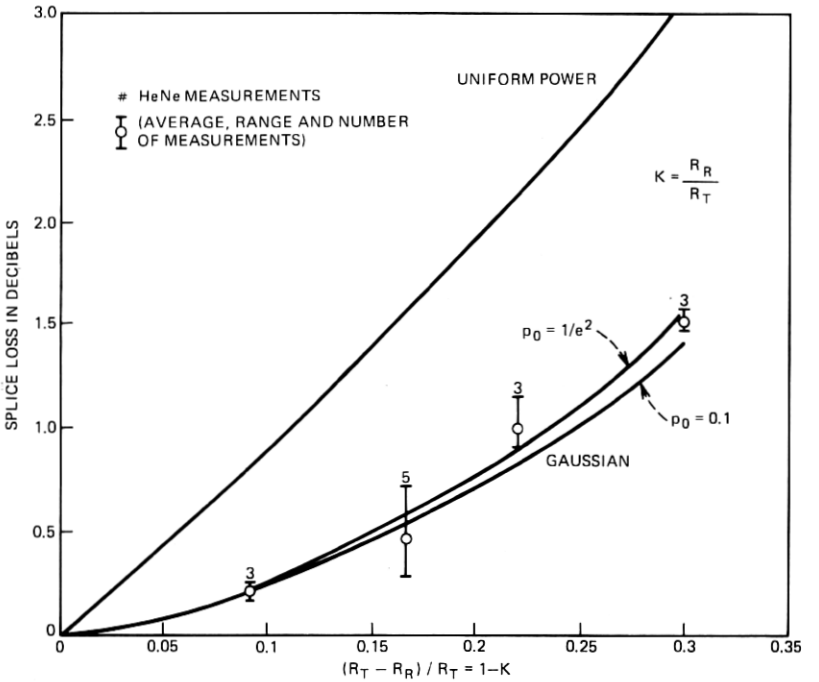

Fig. 7—Loss due to core diameter mismatch.

X. TRANSVERSE OFFSET

Perhaps the most important extrinsic splice parameter is transverse offset (axial displacement). The Gaussian model can be applied to the case of transverse offset; however, some computational difficulties are encountered. Referring to Fig. 8, the area of overlap is divided into region I, where the receiving NA is greater than the transmitting NA, and region II, where the receiving NA is less than the transmitting NA. In region I, $t(\rho)$ is unity, therefore with $R = 1$,

$$T_{\mathrm{I}} = \frac{\int_0^{\cos^{-1}d/2} \int_{d/2\cos\phi}^{1} (1-\rho^2)^2 \, \rho d\rho d\phi}{\int_0^{\pi/2} \int_0^{1} (1-\rho^2)^2 \, \rho d\rho d\phi}. \tag{28}$$

In region II,

$$T_{\mathrm{II}} = \frac{\int_0^{\cos^{-1}d/2} \int_{d/2\cos\phi}^{1} t(q)[1-q^2]^2 \, \rho d\rho d\phi}{\int_0^{\pi/2} \int_0^{1} (1-q^2)^2 \, \rho d\rho d\phi}, \tag{29}$$

where $q = \rho^2 - 2\rho d \cos\phi + d^2$.

Referring to Fig. 8, we note that the line separating regions I and II is a locus of equal NA; therefore, $t(\rho)$ is unity on this line. On the curved boundary of region II, $t(\rho)$ is zero; therefore, the derivative of $t(\rho)$ is infinite at the intersection of these lines. This point must be omitted and, since $t(\rho)$ is steep in the vicinity of this point, a large number of increments are required to evaluate eqs. (28) and (29) numerically.

$$T_{tot} = T_I + T_{II}. \tag{30}$$

If the loss at the splice is desired, (12) is used for $t(\rho)$, and if the total loss including losses required to reestablish steady state is being calculated, then (23) is used.

XI. COMPARISON WITH TRANSVERSE OFFSET DATA

Figure 9 is a comparison of transverse offset data and calculations (*i*) reported by Gloge,[5] (*ii*) using the Gaussian distribution assumption, and (*iii*) using the uniform power assumption. Measurements were made with a GaAlAs laser source and an unbroken long fiber (2 km). After a reference level was established, the fiber was broken approximately in the center and the ends spliced to obtain the reference level again. Offset was introduced and the loss measured 1 km and 2 m after the splice as a function of transverse offset. Figure 9 shows the results for small offsets. Agreement among the Gloge model, the Gaussian model, and measurement data is good for loss at the splice. The Gaussian model also agrees well for the loss occurring in the fiber after the splice.

Figure 10 shows results for large offsets. As compared with actual measurements, the Gaussian model understates the loss through a long

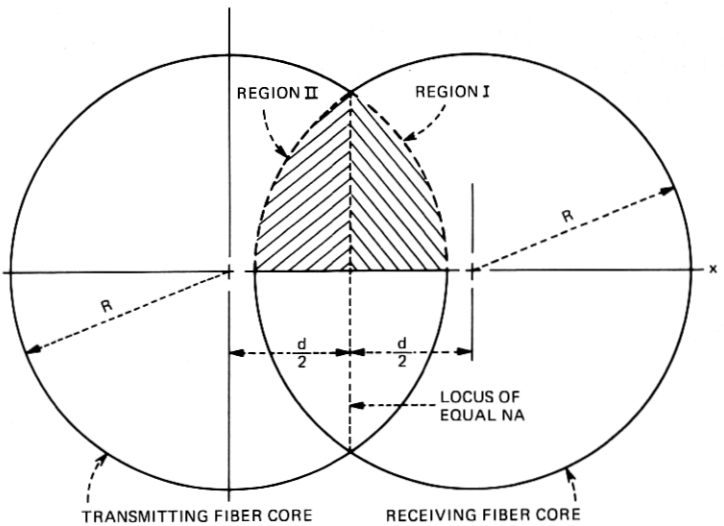

Fig. 8—Regions of overlap for offset fiber cores.

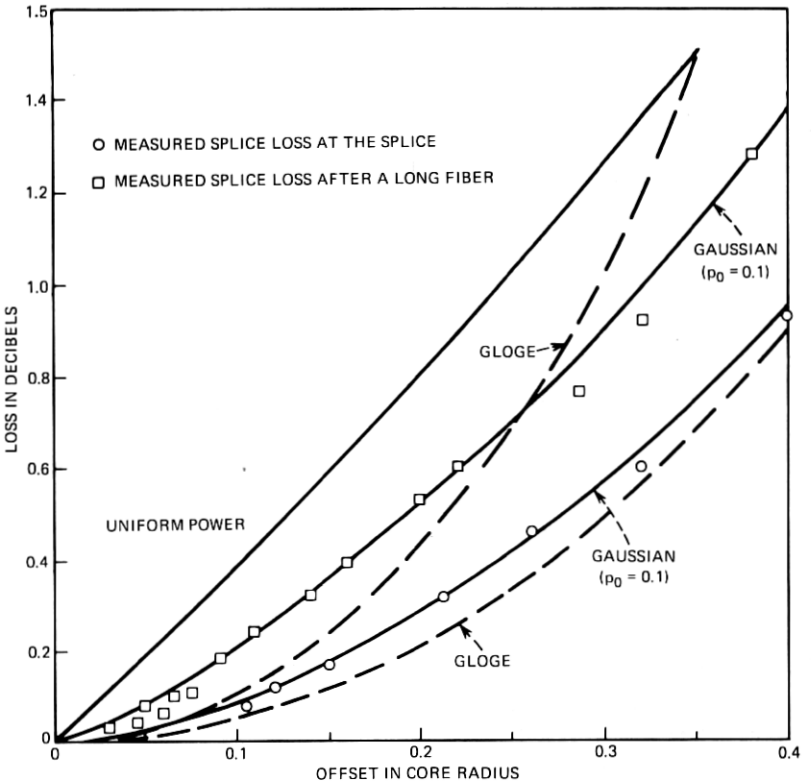

Fig. 9—Loss due to transverse offset.

fiber after the splice for large offsets. The Gaussian model cannot, at present, account for this effect for large offsets.

XII. CONCLUSIONS

A point transmission model has been used to calculate splice loss due to NA mismatch, diameter mismatch, and transverse offset in parabolic-profile fiber splices. Near-field power distributions have also been calculated. Correspondence with measurement data is much improved as compared to calculations using the uniform power distribution model.

The authors again emphasize that the Gaussian power assumption does not obey the laws of ray optics exactly and that this assumption was made primarily due to good correspondence of resulting calculations with measurement data and due to computational considerations. Future work will include the effects of α mismatch and the effects of long fibers after splices with combinations of intrinsic and extrinsic parameter mismatches.

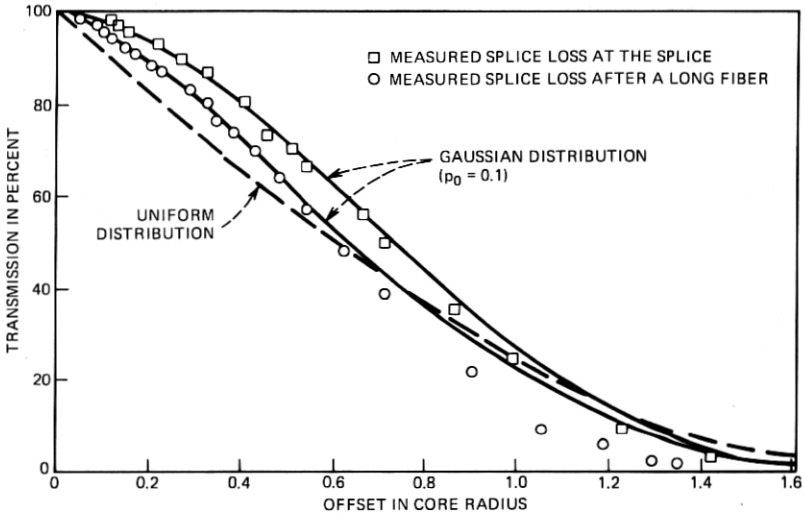

Fig. 10—Transmission vs offset for large offsets.

XIII. ACKNOWLEDGMENT

The authors appreciate the use of diameter mismatch data furnished by M. R. Gotthardt.

REFERENCES

1. F. L. Thiel, "Utilizing Optical Fibers in Communications Systems," Int. Conf. Comm., Conference Record, *II*, Session 32, June 16–18, 1975.
2. Haruhiko Tsuchiya et al., "Double Eccentric Connectors for Optical Fibers," Appl. Opt., *16*, No. 5 (May 1977), pp. 1323–1331.
3. C. M. Miller, "Transmission vs. Transverse Offset for Parabolic-Profile Fiber Splices with Unequal Core Diameters," B.S.T.J., *55*, No. 7 (September 1976), pp. 917–928.
4. D. Gloge and E. A. J. Marcatili, "Multimode Theory of Graded-Core Fibers," B.S.T.J., *52*, No. 9, (November 1973), pp. 1563–1578.
5. D. Gloge, "Offset and Tilt Loss in Optical Fiber Splices," B.S.T.J., *55*, No. 7 (September 1976), pp. 905–916.
6. D. Marcuse, "Loss and Impulse Response of a Parabolic Index Fiber with Random Bends," B.S.T.J., *52*, No. 8 (October 1973), pp. 1423–1437.
7. C. M. Miller, "Realistic Splice Losses for Parabolic Index Fibers," presented at IOOC 1977, Tokyo, Japan, July 18–20, 1977.
8. M. J. Adams et al., "Splicing Tolerances in Graded-Index Fibers," Appl. Phys. Lett., *28*, No. 9 (1 May 1976), pp. 524–526.